OIST OKINAWA INSTITUTE OF SCIENCE AND TECHNOLOGY GRADUATE UNIVERSITY
沖縄科学技術大学院大学

[illegible]	[illegible]
[illegible]	[illegible]
[illegible]	[illegible]
[illegible]	[illegible]
[illegible]	[illegible]
[illegible]	[illegible]
[illegible]	[illegible]
[illegible]	[illegible]

doi: info:doi/10.1038/s41560-019-0406-2

Reduction of lead leakage from damaged lead halide perovskite solar modules using self-healing polymer-based encapsulation

Yan Jiang†, Longbin Qiu†, Emilio J. Juarez-Perez, Luis K. Ono, Zhanhao Hu, Zonghao Liu, Zhifang Wu, Lingqiang Meng, Qijing Wang, Yabing Qi*

Energy Materials and Surface Sciences Unit (EMSSU), Okinawa Institute of Science and Technology Graduate University (OIST) 1919-1 Tancha, Onna-son, Kunigami-gun, Okinawa, 904-0495, Japan

†These authors contributed equally to this work.

* E-mail: Yabing.Qi@OIST.jp (Y.B.Q.)

Nowadays the major factors determining commercialization of lead halide perovskite photovoltaic technology are shifting from solar cell performance to stability, reproducibility, up-scaling, and in particular the concern of Pb leakage during solar cell operation. Here we simulate a realistic scenario that the perovskite solar modules with different encapsulation methods are damaged to a typical extent by mechanical impact (according to the modified FM 44787 standard) and quantitatively measure the lead leakage rates from the damaged modules. We demonstrate that an epoxy resin (ER) based encapsulation method reduces the Pb leakage rate by a factor of 375 compared to the encapsulation method using a glass cover with the UV-resin cured at the module edges. The excellent Pb leakage prevention characteristics is due to the self-healing property of ER and increased mechanical strength. These findings strongly suggest lead halide perovskite photovoltaic products can be used with minimal Pb leakage if appropriate encapsulation is employed.

Lead halide perovskites have garnered considerable attention as efficient light absorbers. Solar cell power conversion efficiency (PCE) has reached 23.7% for single junction perovskite[1] and 28.0% for perovskite silicon tandem structure (two-terminal)[1] on a laboratory scale, already surpassing the other well-established commercial photovoltaic technologies, e.g., multi-crystalline silicon (22.3%) and thin film copper indium gallium selenide (CIGS) (22.9%)[2], suggesting that PCE is no longer a major limiting factor towards commercialization of this novel photovoltaic technology. Lifetime of a perovskite solar cell under operation and the existence of toxic Pb in the perovskite absorber become significant concerns regarding whether and how this technology should be developed.[3-15] Encapsulation is a necessary and widely employed approach to significantly increase the solar cell operational stability by preventing environmental related degradation and enhancing the mechanical strength against external impact. A variety of customized encapsulation methods have been developed for different types of solar cells. For example, a stacked 5-layered structure of glass/ethylene vinyl acetate (EVA)/photovoltaic module/EVA/backsheet is used to encapsulate Si solar panels;[16] a stacked layer of glass/EVA or poly-vinyl butyral (PVB)/photovoltaic module/transparent conductive electrode (TCO) is used to encapsulate CIGS solar panels;[17] a structure of TCO/photoanode/electrolyte/photocathode/TCO is encapsulated by surlyn polymer in dye-sensitized solar cells.[18] Encapsulation methods have been also developed aiming at improving operational stability and reducing the environmental related degradation of perovskite solar cells (PSCs) and modules. Benefiting from decreasing the oxygen and moisture diffusion in the lead halide perovskite absorbers, the T_{80} lifetime of PSCs in ambient condition was improved from 656 h to over 3423 h after encapsulation.[19] Using an EVA encapsulant, PSCs withstood temperature cycling and retained over 90% of their initial performance after 200 temperature cycles.[20] On the other hand, effectiveness of these encapsulation methods against Pb leakage, which is equally important, has not been studied. Similar to Si solar modules, perovskite solar modules for outdoor applications can get damaged or even broken due to natural causes e.g., hailstones, snow and wind loading, fires during usage. The toxic Pb can penetrate

through the damaged region with rain water and contaminate the local environment (Supplementary Fig. 1). Therefore, it is imperative to study the effect of encapsulation on the Pb leakage from damaged perovskite solar modules and to develop an encapsulation method that can effectively minimize the Pb leakage.

In this work, we develop three encapsulation methods for perovskite solar modules, simulate a realistic scenario in which the encapsulated perovskite solar modules are damaged by mechanical impact such as hail impact, and quantitatively measure the Pb leakage rate from the damaged perovskite solar modules, which to our best knowledge is the first attempt in the field. In addition, we use the semi-empirical approximation based on the Noyes-Whitney equation to study the key parameter that determines the lead leakage rate from damaged perovskite solar modules. Furthermore, we characterize the self-healing property of the encapsulation polymer, i.e., epoxy resin (ER), which is used with a multi-stack structure of glass/ER/perovskite solar module/UV-resin/glass to understand how the self-healing property of ER influences the key factor in terms of reducing the Pb leakage rate.

Experimental procedures to assess the Pb leakage

The $Cs_{0.07}FA_{0.93}PbI_3$ perovskite solar modules were prepared according to our reported method (geometry of the perovskite solar module is shown in Supplementary Fig. 2).[21] To ensure the relevance of this study to the real solar cell applications, the perovskite solar modules used here are all working solar modules with reasonable performance. Details of the transmittance and reflectance of the encapsulants and the solar module performance are discussed in the Supplementary Information and shown in Supplementary Fig. 3 and Supplementary Table 1. Four types of configurations, designated as Method A, B, C and D, were studied. In Method A, perovskite solar modules with a structure of FTO/c-TiO_2/$Cs_{0.07}FA_{0.93}PbI_3$/spiro-MeOTAD/Au from top to bottom were used without further encapsulation (Fig. 1a). In Method B, perovskite solar modules were encapsulated by 1 mm thick glass substrates using a UV-resin (XNR5570, NAGASE) at the bottom sides. The UV-resin was coated at the edges of the modules, and

cured under a 400 W UV lamp for 5 min. No encapsulation was performed at the top sides (Fig. 1a). In Method C, perovskite solar modules were first encapsulated at the bottom sides similar to Method B, and then encapsulated by 1 mm thick glass substrates using thermo-compressed surlyn adhesive resin films (DuPont) at the top sides by annealing at 140 ˚C for 10 s (Fig. 1a). The surlyn films show the self-healing property when the heating temperature approaches its melting temperature (Tm), e.g., 85 – 90 ˚C.[22] This encapsulation method has been commonly applied for organic photovoltaics and dye-sensitized solar cells.[18,23] In Method D, perovskite solar modules were first encapsulated at the bottom sides similar to Method B, and then encapsulated by 1 mm thick glass substrates at the top sides using thermo-crosslinking ER films. The ER films also show the self-healing property, i.e., they return from a deformed state (temporary shape) to their original (permanent) shape induced by heating up at temperature higher than the glass transition temperature, Tg.[24,25] As a consequence, the ER films have shown promising applications in manufacturing sensing devices or actuators for medical industries, because of the unique self-healing and easy-processing properties.[26,27] The ER films are formed by mixing diglycidyl ether of bisphenol A type epoxy resin (DGEBA), *n*-octylamine (OA), and m-xylylenediamine (MXDA). The reaction between DGEBA and OA forms linear polymers (Supplementary Fig. 4), which show strong physical crosslinks by tail-to-tail associations among alkyl chains exhibiting the behavior of a physical network.[28,29] By substituting OA with MXDA while maintaining the overall stoichiometric ratio between epoxy and amine, chemical crosslinks are also formed.[31] These chemical crosslinks help improve the mechanical properties of ER, which is evidenced by the increased Tg and Tm.[28, 30] ER has the tendency to self-heal when heated up at temperatures higher than its Tg (i.e., self-healing), but loses its physical strength when heated up at temperatures higher than its Tm. We determined Tg and Tm of the ER films with three different compositions using differential scanning calorimetry (DSC). Based on these results, we selected the particular ER (DGEBA: OA: MXDA = 4: 2: 1) with a Tg of 42 °C and Tm of 88 °C as the encapsulant in encapsulation Method D for our Pb leakage study, because such an ER film shows the self-healing property

and maintains its physical strength at the temperature most relevant to solar cell operation (Supplementary Fig. 5a-d, Video S1-2). However, we claim that the local overheating (known as the hot-spot heating) may occur on the current-limiting cell in a string, causing partial failure of the encapsulation. Therefore re-adjustment of the polymer composition (OA to MXDA ratio) will be needed to increase the Tm, especially at the hot regions. The ER film possesses excellent thermal stability with a thermal degradation temperature of 246.1 °C determined by thermogravimetric analysis (TGA), which is significantly higher than the typical solar cell operating temperature (Supplementary Fig. 6). Activation energy (Ea) corresponding to thermal decomposition of the ER film is 72.6 kJ/mol (Supplementary Fig. 6). To demonstrate the feasibility of this encapsulation method, we also evaluated the cost of the ER layer. The price of the 800-μm-thick ER layer is \$12.3/m^2, which amounts to 4.4% of the total cost of the encapsulated perovskite solar modules[31-34], suggesting that it is a very promising encapsulant from the cost point of view. More detailed information for the cost evaluation can be found in the Supplementary Fig. 7, Supplementary Table 2. The FTO side of the perovskite solar module is designated as the top side allowing light to pass through, and the Au electrode side of the perovskite solar module is designated as the bottom side (Fig. 1a).

To simulate the hail impact, we mechanically broke the encapsulated perovskite solar modules by dropping a metal ball on top of them, similar to the Approval Standard for Rigid Photovoltaic Modules (FM 44787)[35], a standard hail impact test for Si solar panels. We optimized the impact condition using FTO substrates with the similar encapsulation methods to achieve a certain typical damage pattern, i.e., star-shaped microcracks,[36] on damaged encapsulated modules, which can appear in typical-sized PV modules under the standardized test conditions (Supplementary Figs 8 and 9a-h). We assume that the impact intensity is 1 impact per 25 cm^2, which represents an extreme case scenario. Subsequently each damaged perovskite solar module was put in a funnel with a tilt angle of approximately 30˚ with respect to the horizontal direction (Fig. 1b), which is the optimized tilt angle for countries/regions at 35˚ latitude

considering achieving the maximum energy throughout the year.[37] Water was dripped on the damaged region of the perovskite solar modules. Solubility of Pb^{2+} in the rain water strongly depends on the pH value of rain. To simulate the worst scenario, where perovskite solar modules experience a heavy acid rain after being damaged, acid water with a pH value of 4.2 determined by a pH meter was continuously dripped on the damaged part of the module for 1.5 h (Supplementary Fig. 10).[38] Note that the water dripping conditions used in this study are designed with the hope to simulate the actual conditions, but may not be exactly the same as the actual conditions (see details of water dripping tests on damaged perovskite solar modules in the Methods). All the leaked Pb species were collected in the water, which was detected using an inductively coupled plasma mass spectroscopy setup (ICP-MS) to determine the Pb concentration (Fig. 1b).

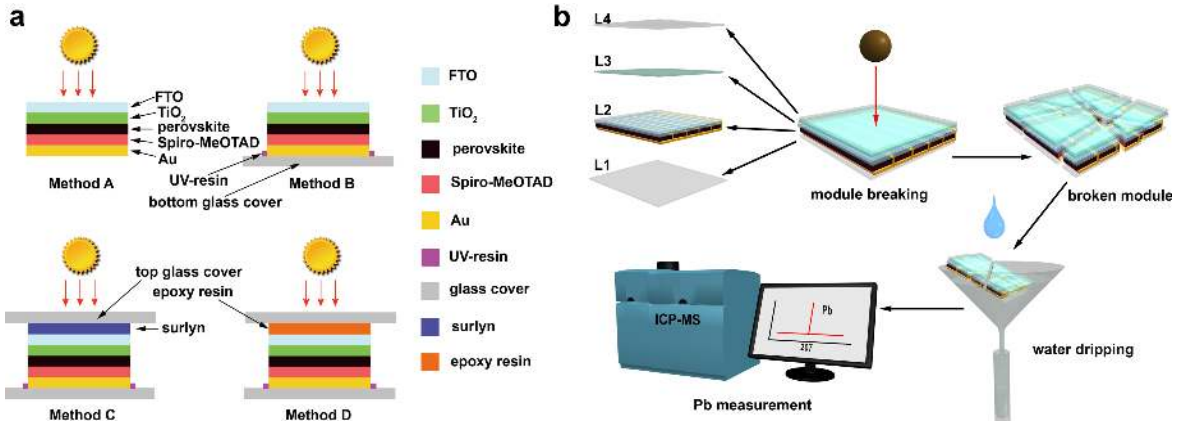

Fig. 1 | Assessment of Pb leakage from damaged perovskite solar modules. (**a**) Schematic drawing showing the encapsulation methods A, B, C and D. (**b**) Schematic drawing showing the experimental procedure to assess the quantity of the toxic Pb leaked from a perovskite solar module that is damaged due to external impact (e.g., hail). Encapsulated perovskite solar modules are mechanically damaged by a metal ball mimicking a standard hail impact test (FM 44787) to achieve a certain typical damage pattern, i.e., star-shaped microcracks,[35] for encapsulated modules. The damaged module is placed in a funnel for water dripping testing to simulate a damaged module under rain. The water is collected and injected into the ICP-MS to measure the Pb concentration. Layer L1 is the bottom encapsulation glass. Layer L2 is the perovskite solar module with the structure of FTO/c-TiO_2/ $Cs_{0.07}FA_{0.93}PbI_3$/spiro-MeOTAD/Au (from top to bottom). Layer L3 is the adhesive resin. Layer L4 is the top glass cover.

The Pb leakage rate from damaged perovskite solar modules

We prepared the first batch of 12 perovskite solar modules (3 perovskite solar modules in each encapsulation method) for the Pb leakage tests (Figs 2a, 2e, 2i for Method A, Figs 2b, 2f, 2j for Method B, Figs 2c, 2g, 2k for Method C and Figs 2d, 2h, 2l for Method D). Under the same impact energy, perovskite solar modules with different encapsulation methods show dramatically different mechanical strength. Perovskite solar modules without encapsulation (Method A) were broken into many pieces (approximately 10 pieces) (Fig. 2m). Perovskite solar modules encapsulated with the Method B were broken into 2-3 large pieces with star-shaped microcracks formed at the hitting position (Fig. 2n). Perovskite solar modules encapsulated with the Methods C and D held in one piece with star-shaped cracks at the hitting position (Figs 2o,p). Hail-typical damages on commercialized solar modules are star-shaped microcracks, suggesting the impact performed on the perovskite solar modules is similar to the real case.[36] We then performed the water dripping tests on the damaged perovskite solar modules. In the real case there could be a period of time, defined as the response time, when the damaged perovskite solar modules are found and replaced / repaired. The damaged perovskite solar modules can experience different weathers, e.g., rainy or sunny during this period of time. We did three experiments to simulate different weather conditions.

In the first experiment, we immediately dripped the acid water (pH = 4.2) on the 4 damaged perovskite solar modules, an undamaged perovskite solar module encapsulated by Method D (designated as Control E) and an FTO substrate (designated as Control F) for 1.5 h with a speed of 5 mL/h to mimic a heavy acid rain right after the hail impact. For the perovskite solar modules after impact, color of some portions of the perovskite solar modules changed from black to yellow after first several minutes of water dripping, demonstrating that perovskite is decomposed to PbI_2.[38] After 1.5 h water dripping, the yellow color is extended to most of the regions for the perovskite solar modules encapsulated by Methods A and B (Figs 2q,r), but only limited to local regions around the star-shaped microcracks for the modules encapsulated by the Methods C and D (Figs 2s,t). The observation demonstrates that the Pb leakage is via the micro-

cracks formed on the damaged FTO substrates for Sample C and D. Variation of the color changing rate for the perovskite solar modules with different encapsulation methods suggests the different decomposition rate of the perovskite films in the perovskite solar modules. The contaminated water that dripped through perovskite solar modules and two control samples was collected to detect the Pb concentration by ICP-MS. Pb concentration in Control F is 0.05 mg/L, which is the background Pb concentration in the water that passes through the system. Sample Control E shows the same Pb concentration as Control F and no color change, revealing that the encapsulation Method D works well. Therefore the Pb leakage in Method C and D is not caused by encapsulation delamination at the module edges. Pb concentrations in the contaminated water are similar for the encapsulation Methods A and B, suggesting that the bottom encapsulation has a negligible effect on Pb diffusion rate under a normal hail impact (Fig. 3a and Table 1). On the other hand, the Pb concentration is drastically decreased to ~14% for the Method C and to ~6% for the Method D compared to the Method A (Fig. 3a and Table 1). This result suggests that a thin adhesive resin film and a top glass cover can substantially enhance the mechanical strength of the perovskite solar modules, result in substantially reduced Pb leakage.

In the second experiment, we heated these decomposed perovskite solar modules at 45 ˚C for 4 h to mimic a reasonable temperature and time range on a sunny day,[39,40] then dripped the acid water again on the damaged modules with a speed of 5 mL/h for 1.5 h to mimic another rain and measured the Pb concentration in the contaminated water. Yellow color extended to almost all the area for perovskite solar modules encapsulated by the Methods A and B (Fig. 2u,v), suggesting that the perovskite decomposed more completely. Size of the yellow color regions is substantially increased for perovskite solar modules encapsulated by the Method C (Fig. 2w) but only slightly increased for the Method D (Fig. 2x). When the comparison is made between the first and second measurements, we found dramatic differences for perovskite solar modules encapsulated by Method D compared to the others. Specifically, Pb concentration ratios before and after annealing are all close to 1 for Sample A, B and C. However, the ratio

substantially decreased to 0.04 for Sample D (Figs 3a, 3b and Table 1). In the case of the Method D, the average Pb concentration on the three samples is as low as 0.03 mg/L (with the background Pb concentration in the water subtracted). The results reveal that our newly developed method (Method D) reduces the Pb leakage significantly better than the incomplete encapsulation methods (Method A and Method B) and the encapsulation method using the surlyn film (Method C), nicely making use of the heating by the sunshine.

On the other hand, Pb concentrion in the second dripping test could also be influenced by the first water dripping test due to differences of the Pb resudual amount. To study the effect of the Pb residual amount on the Pb leakage, we conducted the third Pb leakage test. A second batch of 12 perovskite solar modules (3 perovskite solar modules in each encapsulation method) were damaged at the same impact condition, heated at 45 ˚C for 4 h and water dripped for 1.5 h. The Pb concentration in the contaminated water for each condition is similar to that in the second experiment for all the 4 samples (Fig. 3c, Table 1), revealing that the Pb leakage rates are similar if the Pb residual amount is still sufficient (There is still a lot of yellowish colored PbI_2 as shown in Figs 2u-x).

We calculated the Pb leakage rate according to the Pb concentration in the contaminated solution, and the results are summarized in Table 2. The background Pb concentration obtained for the control Sample E was subtracted for the calculation (see Supplementary Information for the calculation details). The Pb leakage rate without sample heating was extracted from Experiment #1 and with sample heating was extracted from Experiment #3, respectively. The Pb leakage rate is assumed to be approximately constant under each condition. This assumption agrees well with another study of Ag and Zn leakage from organic photovoltaic modules.[41] The encapsulation Method D using a multi-stack structure of glass/ ER/perovskite solar module/UV-resin/glass shows much better performance against Pb leakage than other encapsulation methods. For example, using Method D, the Pb leakage rate is reduced by a factor of

18 without heating by sunshine and by a factor of 375 with heating by sunshine, respectively, compared to the perovskite solar module encapsulated using a glass sheet with UV-resin cured at the module edges (Method B). Although there are different opinions in the literature regarding the environmental impact of Pb contamination caused by perovskite solar modules[38,42-48], it is generally believed that rigorous measures should be taken to prevent Pb from polluting environment. Because of the excellent performance against Pb leakage, our newly developed encapsulation method D is expected to help achieve this goal.

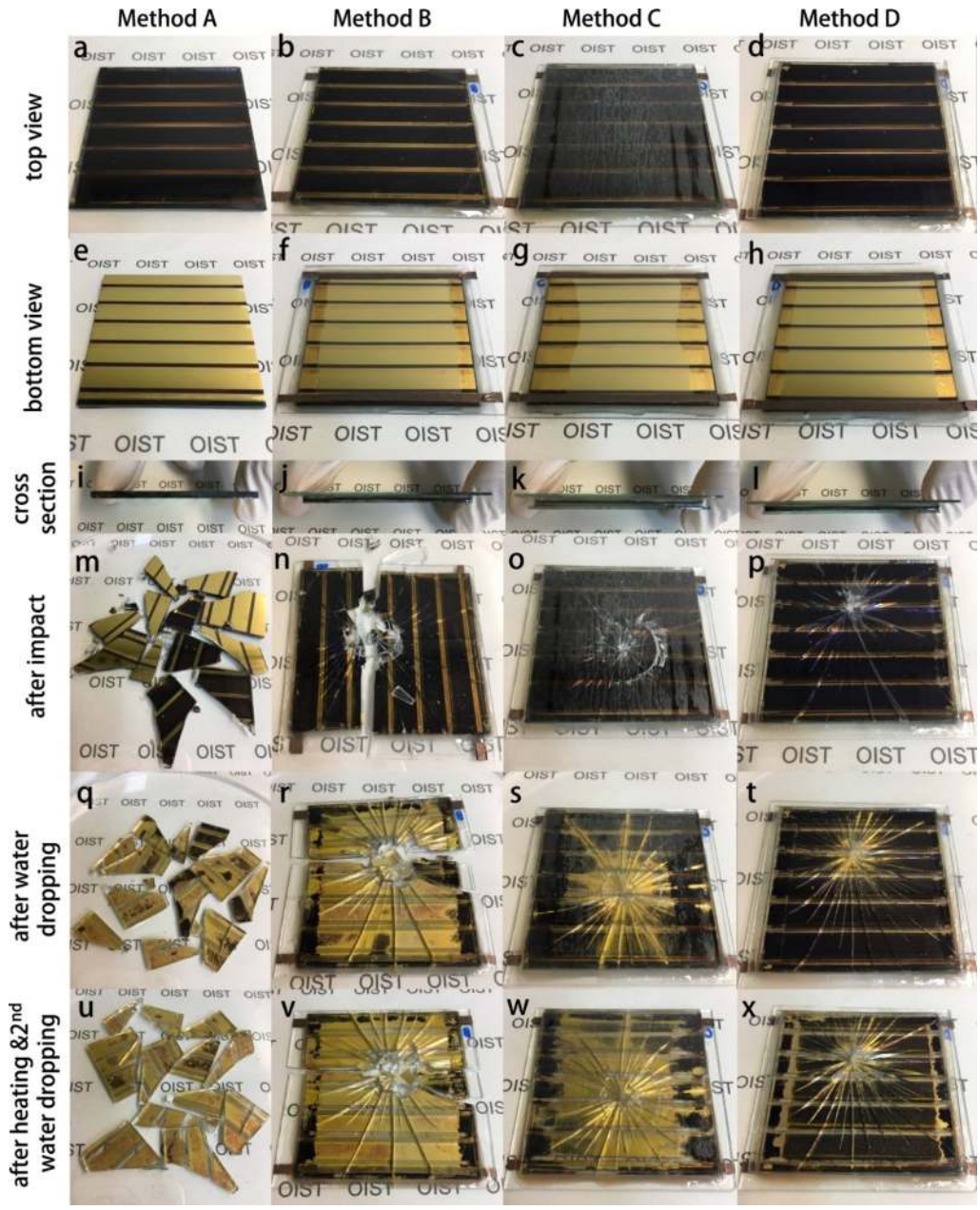

Fig. 2 | **Photographs of perovskite solar modules.** (**a-l**) Perovskite solar modules before being intact. (**m-p**) Perovskite solar modules after impact. (**q-t**) perovskite solar modules after first water dripping test. **(u-x)** perovskite solar modules after first water dripping test, heating at 45 ˚C for 4h and second water dripping test. (**a,e,i,m,q,u**) the perovskite solar module without encapsulation (Method A), encapsulated with (**b,f,j,n,r,v**) Method B; (**c,g,k,o,s,w**) Method C and (**d,h,l,p,t,x**) Method D. Different perovskite solar module encapsulation methods lead to different degrees of perovskite decomposition under the same impact and water dripping conditions.

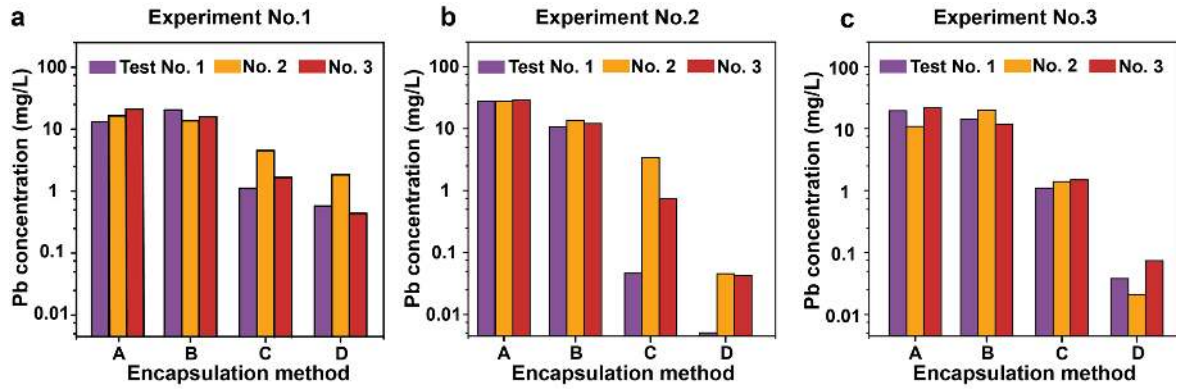

Fig. 3 | **Pb leakage concentration in the contaminated water.** (**a**), experiment No. 1. Water dripping tests are conducted on the perovskite solar modules. Pb concentration in the contaminated water was detected by ICP-MS. (**b**), experiment No. 2. The perovskite solar modules were water dripped, heated at 45 ˚C for 4h to simulate the sunny weather, and water dripped for the second time. Pb concentration in the second dripping water was tested. (**c**), experiment No. 3. The perovskite solar modules were heated at 45 ˚C for 4h and water dripped. The Pb concentration was tested. Three samples, named as Test No.1, No.2 and No.3 were tested at each condition. The Pb leakage concentration is substantially influenced by the encapsulation methods.

Table 1 | **Pb concentration in dripping water passing through damaged perovskite modules**

Experiment No.	Test condition	Pb concentration in the last dripping water (mg/L or ppm)					
		Method A	Method B	Method C	Method D	Control E	Control F
1	Water dripped	17±3	16±3	<2	<0.9	5×10^{-2}	5×10^{-2}
2	Water dripped, heated and water dripped again	27.5±0.6	12±1	<1	$<8 \times 10^{-2}$	-	-
3	Heated and water dripped	17±4	15±3	<1.3	$<9 \times 10^{-2}$	-	-

Water dripping test is conducted on (Control E) an undamaged perovskite solar module encapsulated by Method D and (Control F) an FTO substrate. No metal ball impact is performed for Samples control E and Control F. For methods A, B, C and D, three samples are tested at each condition. Data shown here are the average values. The error bars represent the standard deviations calculated based on the measurement results collected from 3 different samples.

Table 2 | **Pb leakage rate without and with the heating treatment**

	Method A	Method B	Method C	Method D
Pb leakage rate without heating (mg/(h × m^2))	34±6	32±6	<4	<1.8
Pb leakage rate with heating (mg/(h × m^2))	34±8	30±6	<2.6	$<8\times 10^{-2}$

Pb leakage rate calculation: Pb ions are assumed to leak at a constant rate under each condition (i.e., using different encapsulation method and heating condition) when the Pb residual amount was sufficient to maintain the Cs at constant value (A_e, D, d and C_b values do not change with

time). The error bars represent the standard deviations calculated based on the measurement results collected from 3 different samples. See Supplemental Information for the calculation details.

Simulated assessment of the Pb leakage from damaged perovskite solar modules

To understand how the encapsulation methods influence the Pb leakage rate, here we use the semi-empirical approximation based on the Noyes-Whitney equation, which has been used by Celik et al. to study the metal leakage from damaged perovskite solar cells.[45]

$$\frac{\mathrm{d_m}}{\mathrm{d_t}} = \mathrm{A}_e \left(\frac{\mathrm{D}}{\mathrm{d}}\right)(\mathrm{C}_s - \mathrm{C}_b) \quad (1)$$

where m is the mass of the dissolved Pb, t is the diffusion time, A_e is the effective exposure area that Pb exposed to the solvent, D is the diffusion coefficient of Pb^{2+} ion, d is the thickness of the encapsulation boundary layer (polymer and the top glass cover), C_s is the saturated mass concentration at the surface of the solution and C_b is mass concentration in the bulk solution. Because values of the parameters are known either from literature (D, C_s and C_b,)[45] or from our experimental results (d and dm/dt), we are able to calculate the value of A_e, which is a key factor influencing the Pb leakage rate. Details of calculation are shown in Supplementary Table 3. For the samples without heating treatment (experiment No. 1), A_e is similar for Sample A (3.7 cm^2) and Sample B (3.4 cm^2), and substantially decreased for Sample C (0.49 cm^2) and Sample D (0.33 cm^2). The reduction of A_e for Sample C and D comparing to Sample A and B is because of the improved mechanical strength by putting the encapsulation polymer and the top glass cover on the perovskite solar module. For the samples with heating treatment, A_e of Samples A, B and C do not change after the heating treatment (Supplementary Table 3). On the other hand, A_e of Sample D after heating treatment is dramatically reduced (1.3×10^{-2} cm^2) comparing with the same sample without heating (0.33 cm^2). We think the substantially reduced A_e for Sample D after heating is due to addition of the ER layer between FTO and top glass cover. The ER film is known to possess the self-healing property in crushed microstructure and damaged surface after heating, and therefore can prevent water from penetration into the damaged perovskite solar modules.[25] In sharp contrast, the A_e for Sample C does not reduce after

heating because the heating temperature is too low to activate the self-healing property of the surlyn film.[22]

Self-healing properties of the epoxy resin encapsulant

To reveal the self-healing phenomenon of Method D during solar cell operation, we then focus on characterization of the chemical and physical property of the ER film under the heating treatment that can be caused by sunshine. We drop cast the ER films (DGEBA: OA: MXDA = 4: 2: 1) on glass slides and let them cure at 70 °C for 10 min. The films were cut with a knife to achieve mechanical damages with a width of approximately 40 μm and then heated at 45 ˚C for 4 h (Fig. 4a). We studied the effect of heating on the surface hydrophobicity property of ER by conducting water contact angle (CA) measurements on the ER film before cutting, after cutting but before heating, and after cutting and after heating. Water CA is 106.6±0.6˚ for the pristine ER film and 24.6±0.4˚ for the film with microcrack at the cutting region (Figs 4b,c). After heating, hydrophobicity at the cutting region is almost completely recovered showing a CA of 104±2˚ (Fig. 4d). The results reveal that the recovery of the surface hydrophobicity after heating leads to reduction of A_e. Furthermore, we studied the morphology of the pristine ER films (3 samples) without cutting, after cutting but before heating, and the ER films after cutting and 4 h heating by scanning electron microscopy (SEM). The Surlyn films (3 samples) used as control samples were melt on the glass slides at 120 °C for 2 min, which formed solid films after they cooled down to room temperature. The ER films are relatively flat before cutting (Fig. 4e), while deep valleys are clearly visible on both the ER films and the Surlyn films after cutting (Figs. 4f,h, Supplementary Fig. S11). After the heating treatment, the valley on the ER films are re-filled by forming micro-structured ER (Figs. 4g,i). On the other hand, the valley on the Surlyn film remains almost unchanged (Supplementary Fig. S11). These results suggest that only the ER film shows the self-healing property under such a heating condition. To quantitatively study the self-healing property at 45 °C, the cut depth, defined as the height difference between the baseline and the bottom of the valley at the cutting region, was measured by a profilometer at different heating times

(the raw data can be found in Supplementary Figs 12-14, and Supplementary Table 4). We plotted a figure showing the normalized cut depth, i.e., the cut depth value after a certain time of heating normalized with respect to the initial cut depth value upon fresh cutting, as the function of the heating time. We observe a clear reduction of the normalized cut depth after 1 h, which further decreases slightly after heating for 4 h (Fig. 4j). This is another piece of evidence confirming that the ER films heal after heating at 45 °C. Note that although the heating temperature of 45 ˚C is selected in this study which represents a conservative case, solar cells or modules can get even hotter during normal operation. Therefore, 85 ˚C is selected for damp heat test and thermal cycle test in the IEC 61215 standard.[49] It is necessary to study the self-healing property and stability of the ER film at higher temperatures to evaluate the durability of such an encapsulant. We deposited 6 ER films on glass slides, cut and heated them at 65 ˚C and 85 ˚C, respectively (3 samples for each heating condition). The cutting region heals much faster than the sample heated at 45 ˚C (Figs 4j, see the details in Supplementary Figs 12-14 and Supplementary Table 4). Especially for the sample heated at 85 ˚C, almost no cutting trace is observed after 1 h (Fig. 4j). These results suggest that the self-healing characteristics are more pronounced at elevated temperatures. On the basis of these results, we can safely conclude that both the damaged hydrophobicity and crushed microstructure formed on the ER film during the hail impact recover after heating, resulting in substantially reduced A_e. As a consequence, the ER film can effectively prevent water from penetration into the perovskite solar modules via star-shaped microcrack region leading to substantially reduced Pb leakage.

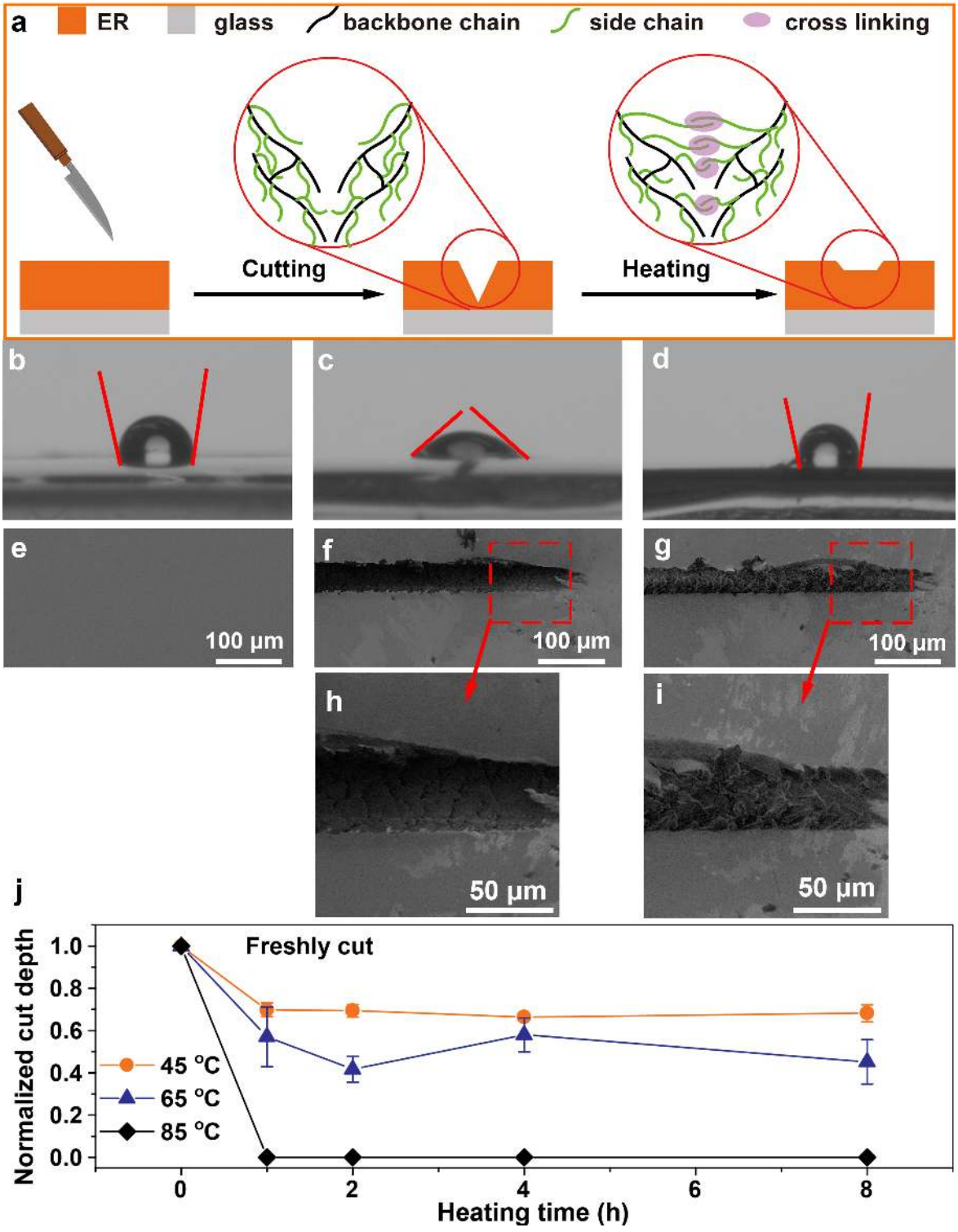

Fig. 4 | **Self-healing property of the epoxy resin encapsulant.** (**a**) Schematic drawing showing the self-healing process of the epoxy resin. The side-view photos showing the water contact angle on (**b**) the

pristine ER film, (**c**) the film after cutting, and (**d**) the film after cutting and heating at 45 ˚C for 4 h. The top-view SEM images showing (**e**) the pristine ER film before cutting, (**f**) the film after cutting but before heating, and (**g**) the film after cutting and heating at 45 ˚C for 4 h. (**h**) The SEM image showing the enlarged region marked in (**f**). (**i**) The SEM image showing the enlarged region marked in (**g**). (**j**) The normalized cut depth as a function of heating time under 3 different heating temperatures (45 °C, 65 °C, and 85 °C). The cut depth is defined as the height difference between the baseline and the bottom of the valley at the cutting region (the raw data can be found in Supplementary Figs 12-14, and Supplementary Table 4). The normalized cut depth (i.e., the y axis value of Figure 4**j**) is the cut depth value after a certain time of heating normalized with respect to the initial cut depth value upon fresh cutting. For example, for any heating temperature, the normalized cut depth equals to 1 at the heating time of 0 h (i.e., in the state of being freshly cut and without any heating). The error bars represent the standard deviations calculated based on the measurement results collected from 3 different samples.

Effect of the weather condition on the Pb leakage with different encapsulation

The damaged perovskite solar modules can experience different weather conditions within the response time, which can affect the lead leakage amount. To comprehensively assess the Pb leakage amount for different encapsulation methods, 4 possible weather conditions and 3 response times, namely 12 h (fast), 72 h (medium) and 720 h (slow), are simulated, amounting to a total number of 56 conditions. We calculate the Pb leakage amount based on the leakage rate (Supplementary Table 5). Under a normal weather condition when a short rain lasts for 4 h, the Pb leakage amount is similar for encapsulation Methods A (140 mg/m^2) and B (130 mg/m^2) and decreased to C (16 mg/m^2) and D (7 mg/m^2) at both 12 and 72 h response time (Figs 5a, 5e). Comparing with the work by Hailegnaw et al., i.e., when ~70% of Pb mass loss is observed after 1 h dripping test[38], the Pb leakage rate is much slower even for Sample A (~26% Pb mass loss in 4 h). The different Pb leakage rates are due to different sample structures (a complete device with the structure of FTO/TiO_2/perovskite/Spiro-MeOTAD/Au vs. a bare perovskite film) and different water dripping directions (the FTO side versus the perovskite side). In a serious condition when a heavy rain lasts for 72 h, the Pb leakage amount is increased for all the encapsulation methods. For example, The Pb leakage amount reaches the maximum value (540 mg/m^2) for Methods A and B at 72 h, increases from 48 mg/m^2 at 12 h to 290 mg/m^2 at 72 h for Method C and increases from 22 mg/m^2 at 12 h to 130 mg/m^2 at 72 h for Method D (Figs 5b, 5f). Heating from the sunshine makes drastically different

Pb leakage amounts between perovskite solar modules encapsulated employing an ER layer (Method D) and the other methods. If it rains for the first 4 h, with sun rises for 4 h in total and rains again starting at 48 h for 24 h, a huge Pb leakage amount variation is shown comparing to a fast and a medium response time for encapsulation Method A (140 mg/m^2 at 12 h and 540 mg/m^2 at 72 h), B (130 mg/m^2 at 12 h and 540 mg/m^2 at 72 h) and C (16 mg/m^2 at 12 h and 78 mg/m^2 at 72 h), but show very little effect for encapsulation Method D (7 mg/m^2 at 12 h and 9 mg/m^2 at 72 h) (Figs 5c, 5g). Under an extreme whether condition when the damaged perovskite solar modules experience a sunny weather for 4 h and multiple rains for 200 h and a slow response time of 720 h, the Pb leakage amount reaches the maximum value (540 mg/m^2 at 720 h) for encapsulation Methods A, B and C (Fig. 5d). On the other hand, encapsulation Method D shows an extremely small quantity of Pb (16 mg/m^2 at 720 h), suggesting the outstanding protection of Method D in preventing the Pb from leakage. We interpret the data as follows.

(I) Encapsulation methods can dramatically influence the Pb leakage amount from a damaged perovskite solar module. A complete encapsulation Method D using a multi-stack structure of glass/ER/perovskite solar module/UV-resin/glass reduces the Pb leakage amount significantly better than other encapsulation methods (Figs 5a-g).

(II) Weather condition is another factor influencing the Pb leakage amount. Shorter time of rainfall results in a lower Pb leakage amount; Sunny weather right after the module being damaged shows very little beneficial effect for Methods A, B, C, but drastically reduce the Pb leakage amount in the case of Method D (Figs 5c, 5d, 5g).

(III) Response time also influences the Pb leakage amount. A longer response time results in a larger Pb leakage amount.

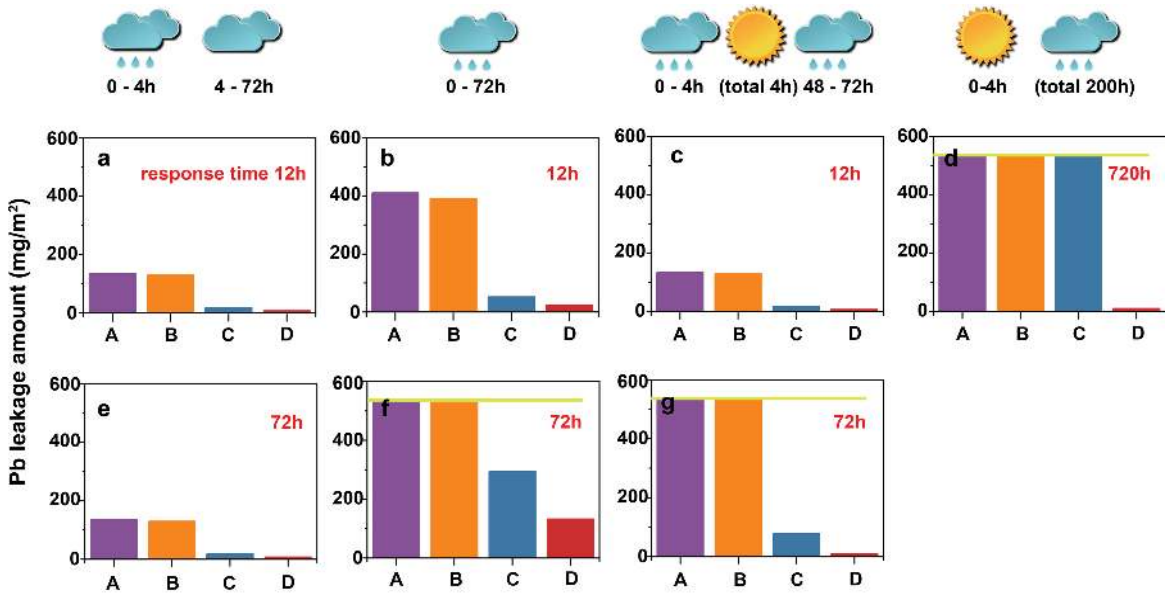

Fig. 5 | **Effect of weather condition on Pb leakage with different encapsulation methods.** (**a,e**), it rains for the first 4 h and cloudy until 72 h. (**b,f**), it rains constantly for 72 h. (**c,g**), it rains for the first 4 h, with sun rises for 4 h in total and rains again starting at 48 h for 24 h. (**d**), it is sunny for the first 4 h and start for multiple rains for 200 h in total in 720 h. Yellow lines in (**d,f,g**) represent the maximum Pb amount that can leak from a damaged perovskite solar module. 4 different weather conditions are shown at the top of figure and 3 different response times (12 h, 72 h and 720 h) are labeled in red color in each figure.

Conclusions and outlook

In summary, we quantitatively measured the lead leakage from the damaged perovskite solar modules without encapsulation and as well as with 3 different encapsulation methods. The Pb leakage amount is strongly dependent on the encapsulation methods, weather condition and response time. With carefully designed experiments to simulate realistic conditions, we demonstrate that our customized encapsulation method with a multi-stack structure of glass/ER/perovskite solar module/UV-resin/glass which shows excellent performance against Pb leakage from the damaged perovskite solar modules. The results shed light on effective methods to solve the potential toxicity concern of Pb-based metal halide perovskite photovoltaic technology. Further works that can help further resolve this issue include establishment of perovskite photovoltaic industry standard, optimization of the perovskite solar cell encapsulation

methods, development of the rigorous maintenance, emergency processing and recycling programs to meet the safety requirement of this technology.

Methods

Perovskite solar module fabrication. Perovskite solar modules, each containing 6 sub-cells connected in series with a total active area of 12.0 cm^2, were fabricated according to our reported methods.[21] The active area of the perovskite solar modules is determined by the overlap regions of FTO and Au electrode (Supplementary Fig. 1). Patterned FTO glasses (7-8 Ω/□, Opvtech.) were cleaned by sequentially sonicating in deionized water, ethanol and acetone as substrates. UV-Ozone treatment was performed on the substrates just before use. A 40 nm c-TiO_2 layer was deposited via magnetron sputtering at 180 W with a mask. A 550 nm $Cs_{0.07}FA_{0.93}PbI_3$ perovskite layer was deposited on the TiO_2 layer via a three-step process. First, a PbI_2·DMSO film was spin-coated using 1:1 molar ratio of lead iodide (TCI, 99.99%) and DMSO (99.9%, Sigma-Aldrich) in DMF (99.8%, Sigma-Aldrich) (1.3 M) and annealed at 100 °C for 5 min; Second, the PbI_2·DMSO film is converted to $FAPbI_3$ via CVD deposition of FAI (Dyesol) under a low vacuum (1 Torr) for 2.5 h with the source and substrate zone temperature of 190 °C and 155 °C, respectively. Third, the as prepared $FAPbI_3$ film is immersed in the cesium acetate (99.9%, Sigma-Aldrich) in IPA (98%, Sigma-Aldrich) solution (2mg/mL) for 3 s at room temperature in a N_2 filled glovebox, followed by annealing at 150 °C for 20 min in air. A 200 nm spiro-MeOTAD layer was spin-coated on the $Cs_{0.07}FA_{0.93}PbI_3$ perovskite layer with a solution containing 72.3 mg spiro-MeOTAD (Merck), 28.8 µL of 4-*tert*-butylpyridine (98%, Sigma-Aldrich) and 17.5 µL of lithium bis(trifl uoromethanesulfonyl)imide (Li-TFSI) solution (520 mg Li-TSFI in 1 mL acetonitrile (Sigma-Aldrich, 99.8 %)) in 1mL of chlorobenzene. The perovskite and spiro-MeOTAD layers are partially removed by mechanical scratch using a second mask. A 120 nm gold electrode was deposited via thermal evaporation (0.01-0.08 nm/s) on the spiro-MeOTAD layer using a third mask.

Characterization. Transmittance and reflectance of the substrates with different top encapsulation methods was characterized by UV/Vis spectrometer (JASCO Inc., V-670). Surface roughness measurements on the surlyn and ER films were conducted using a profilometer (Dektak XT, Bruker). Morphology of the cutting region of surlyn and ER films was measured by field emission scanning electron microscopy (Helios NanoLab G3 UC, FEI). The water contact angle was obtained by a drop shape analyzer (krüss GmbH). Tg and Tm of the ER films with different compositions were measured using a DSC (DSC 8500, Perkin Elmer) with a scan rate of 20 °C/min from -10 to 100 °C. An Indium reference sample was measured for calibration. Thermal stability of the films was determined by TG measurements using a Netzsch TG-DTA2000SE thermal analyzer. Measurements were performed in aluminum crucibles under a stationary ambient air atmosphere with a scan rate of 15, 20 and 25 K/min from room temperature to 600 °C. Solar cell performance was measured under AM 1.5 G one-sun illumination (100 mW/cm^2) using a solar simulator (Newport Oriel Sol A) and Keithley 2420 source meters. Intensities of the solar simulators were calibrated with a calibrated silicon detector (Oriel Instruments Model 91150V). All the J-V characteristics were carried out in ambient (RH ~ 60%) at room temperature. Scan rates were 0.2 V/s in the forward to backward direction. 10 s pre-illumination and no pre-bias were applied for the measurement. Pb concentration in the dripping water was detected using an inductively coupled plasma mass spectroscopy (Thermal Scientific, element 2).

Perovskite solar module encapsulation. Perovskite solar modules were encapsulated in Method A, B, C and D (Fig. 2a). In Method A, perovskite solar modules with a structure of FTO/c-TiO_2/ $Cs_{0.07}FA_{0.93}PbI_3$/spiro-MeOTAD/Au from top to bottom were used without further encapsulation. In Method B, perovskite solar modules were encapsulated by 1 mm thick glass substrates using a UV-resin (XNR5570, NAGASE) at the bottom sides. The UV-resin was coated at the edges of the modules, and cured under a 400 W UV lamp for 5 min. No encapsulation was performed at the top sides. In Method C, perovskite solar modules were first encapsulated at the bottom sides similar to Method B,

and then encapsulated by 1 mm thick glass substrates using thermos-compressed surlyn adhesive resin films (DuPont) at the top sides by annealing at 140 ˚C for 10 s. In Method D, perovskite solar modules were first encapsulated at the bottom sides similar to Method B, and then encapsulated by 1 mm thick glass substrates at the top sides using thermo-crosslinking SHP films by mixing diglycidyl ether of bisphenol A type epoxy resin (Sigma-Aldrich), *n*-octylamine (Sigma-Aldrich), and m-xylylenediamine (Sigma-Aldrich) with a molar ratio of 4:2:1 and annealing at 70 ˚C for 10 min. Thickness of the surlyn adhesive resin film is 80 µm. We optimized thickness of the SHP film to be approximately 80 µm by performing a proper pressure during the annealing process for comparison.

Impact tests of perovskite solar modules. Perovskite solar modules were damaged mechanically similar to the Approval Standard for Rigid Photovoltaic Modules (FM 44787)[35], where a metal ball (45 mm in diameter, 358 g) was dropped from a certain height onto the perovskite solar modules. Because the size of our perovskite solar module (25 cm^2) was much smaller than the commercial Si solar panel which is used for standard hail impact test, e.g., FM 44787, we optimized the impact condition using FTO substrates with the similar encapsulation methods to achieve a certain typical damage pattern, i.e., star-shaped microcracks,[36] on damaged encapsulated modules. Such damage patterns can appear in typical-sized PV modules in the standardized test conditions (Supplementary Figs 8 and 9). The breaking tests were performed on FTO substrates with the 4 types of encapsulation methods including FTO substrates without encapsulation (designated as A); FTO substrates encapsulated with a 1 mm thick glass using a UV-resin on the one side and a SHP film on the other side (designated as B); FTO substrates encapsulated with a 1 mm-thick glass on one side, a 80 µm-thick surlyn film and 1 mm-thick glass on the other side (designated as C); FTO substrates encapsulated with a 1 mm-thick glass on one side, a 80 µm-thick SHP film and 1 mm-thick glass on the other side (designated as D). When the distance was 10 cm, FTO substrates without encapsulation or top cover (Method A) broke into many pieces (Supplementary Fig. 9e). FTO substrates encapsulated with Method B broke into 2-3 main pieces with star-shaped microcracks formed at the hitting position (Supplementary Fig. 9f). FTO substrates encapsulated with Methods C and D remained in one piece and showed star-shaped microcracks at the hitting position (Supplementary Figs 9g,h). We fixed the height to be 10 cm for hitting the perovskite solar modules. We assume that the impact density is 1 impact per 5 cm × 5 cm, which represents an extreme case scenario. Based on this assumption, the averaged distance between the two adjacent impacts is close (5 cm). Therefore, after the formation of the first crack, an even higher impact for the adjacent second crack may be required to achieve a similar crack pattern of the first crack because the broken module may yield better strength to the second impact stresses. The actual situation could be that the Pb leakage rate per area is not as high as the results we have obtained.

Water dripping tests on damaged perovskite solar modules. Each of the damaged perovskite solar modules (encapsulated by A, B, C, D) was placed in the in a funnel with ~30˚ relative to ground for the water dripping tests (Supplementary Fig. 10). Glass slides were used to hold the broken pieces of the perovskite solar modules encapsulated by Method A and B at the same angle for the test. Deionized water with pH of 4.2 determined by a pH meter was continuously dripped on a bare FTO glass substrate for detection of the Pb background and the damaged part of the perovskite solar modules using a syringe pump at 5 mL/h for 1.5 h. The rain contact area, defined as the area that a water drop actually spread on the damaged glass cover, is around 1 cm^2 according to statistical results of 50 water drops on a glass cover. (Supplementary Fig. 10) Therefore the rain intensity is 50 mm/h, which is in the typical heavy rain range.[38, 50] The Pb contaminated water was collected by centrifuge tubes. This method considers the rain intensity and the drop size and assumes that the rainfall is uniformly distributed in the investigated region. It does not consider the impact energy of the rain drops, therefore may not be exactly the same as the actual condition. We are aiming at studying the worst scenario of Pb leakage from damaged perovskite solar modules. However, the actual Pb leakage rates are expected to change dependent on the module size, hail size, impact density, rainfall rate, etc.

References

1. *Best Research Cell Efficiencies* (NREL, 2019); https://www.nrel.gov/pv/cell-efficiency.html *and* https://www.nrel.gov/pv/module-efficiency.html
2. Green, M. A., Hishikawa, Y., Dunlop, E. D., Levi, D. H., Hohl-Ebinger, J. & Ho-Baillie, A. W. Y. Solar cell efficiency tables (version 53). *Prog. Photovolt. Res. Appl.* **27**, 3–12 (2019).
3. Correa-Baena, J. et al. Promises and challenges of perovskite solar cells. *Science* **358**, 739-744 (2017).
4. Park, N.-G., Grätzel, M., Miyasaka, T., Zhu, K. & Emery, K. Towards stable and commercially available perovskite solar cells. *Nat. Energy* **1**, 16152 (2016).
5. Rong, Y. et al. Challenges for commercializing perovskite solar cells. *Science* **361**, eaat8235 (2018).
6. Christians, J. A. et al. Tailored interfaces of unencapsulated perovskite solar cells for >1,000 hour operational stability. *Nat. Energy* **3**, 68-74 (2018).
7. Ono, L. K., Qi, Y. B. & Liu, S. Z. Progress toward stable Lead Halide Perovskite Solar Cells. *Joule* **2**, 1961-1990 (2018).
8. Park, N., Huang, J., & Qi, Y. B. Themed issue on perovskite solar cells: research on metal halide perovskite solar cells towards deeper understanding, upscalable fabrication, long-term stability and Pb-free alternatives. *Sustain. Energy Fuels* **2**, 2378-2380 (2018).
9. Juarez-Perez, E. J., Ono, L. K., Maeda, M., Jiang, Y., Hawash, Z. & Qi, Y. B. Photo-, Thermal-decomposition in Methylammonium Halide Lead Perovskites and inferred design principles to increase photovoltaic device stability. *J. Mater. Chem. A* **6**, 9604-9612 (2018).
10. Wang, S., Jiang, Y., Juarez-Perez, E. J., Ono, L. K., & Qi, Y. B. Accelerated degradation of methylammonium lead iodide perovskites induced by exposure to iodine vapour *Nat. Energy* **2**, 16195 (2016).
11. Juarez-Perez, E. J., Hawash, Z., Raga, S. R., Ono, L. K., & Qi, Y. B. Thermal degradation of $CH_3NH_3PbI_3$ perovskite into NH_3 and CH_3I gases observed by coupled thermogravimetry - mass spectrometry analysis. *Energy Environ. Sci.* **9**, 3406–3410 (2016).
12. Rajagopal, A., Yao, K. & Jen, A. K. Toward Perovskite Solar Cell Commercialization: A Perspective and Research Roadmap Based on Interfacial Engineering. *Adv. Mater.* **30** 1800455 (2018).
13. Ju, M. et al. Toward Eco-friendly and Stable Perovskite Materials for Photovoltaics. *Joule* **2**, *1231-1241* (2018).
14. Abate, A. Perovskite Solar Cells Go lead Free. *Joule* **1**, 659-664 (2018).
15. Shi, Z. J. et al. Lead-Free Organic-Inorganic Hybrid Perovskites for Photovoltaic Applications: Recent Advances and Perspectives. *Adv. Mater.,* **26**, 1605005 (2017).
16. Jiang, S., Wang, K., Zhang, H., Ding, Y. & Yu, Q. Encapsulation of PV Modules Using Ethylene Vinyl Acetate Copolymer as the Encapsulant. *Macromol. React. Eng.* **9**, 522–529 (2015)
17. *Manufacture of a CIGS solar module* (Soltecture, 2018); http://www.soltecture.com/technology/production-since-2003/manufacturing-processes.html.
18. Hirata, M. K., Freitas, J. N., Santos, T. E. A., Mammana, V. P. & Nogueira, A. F. Assembly Considerations for Dye-Sensitized Solar Modules with Polymer Gel Electrolyte. *Ind. Eng. Chem. Res.* **55**, 10278−10285 (2016).
19. Wang, Z. et al. Efficient and Air-Stable Mixed-Cation Lead Mixed-Halide Perovskite Solar Cells with n-Doped Organic Electron Extraction Layers. *Adv. Mater.* **29**, 1604186 (2017).
20. Cheacharoen, R. et al. Design and understanding of encapsulated perovskite solar cells to withstand temperature cycling. *Energy Environ. Sci.* **11**, 144-150 (2018).
21. Jiang, Y. et al. Combination of Hybrid CVD and Cation Exchange for Upscaling Cs-Substituted Mixed Cation Perovskite Solar Cells with High Efficiency and Stability. *Adv. Funct. Mater.* **28**, 1703835 (2018).
22. Kalista, Jr. S. J, Self-healing of Thermoplastic Poly(ethylene-co-methacrylic Acid) Copolymers Following Projectile Puncture. Masters Thesis, Virginia Tech (2003).
23. Lertngim, A. et al. Preparation of Surlyn films reinforced with cellulose nanofibres and feasibility of applying the transparent composite films for organic photovoltaic encapsulation. *R. Soc. open Sci*. **4**, 170792 (2017).
24. Hager, M. D., Greil, P., Leyens, C., Zwaag, S. V. D. & Schubert, U. S. Self-Healing Materials. *Adv. Mater.* **22**, 5424-5430 (2010).
25. Lv, T. et al. Self-Restoration of Superhydrophobicity on Shape Memory Polymer Arrays with Both Crushed Microstructure and Damaged Surface Chemistry. *Small* **13**, 1503402, (2017).
26. Rousseau, I. A. Challenges of Shape Memory Polymers: A Review of the Progress Toward Overcoming SMP's Limitations. *Polym. Eng. Sci*. **48**, 2075-2089 (2008).

27. Lantada, A. D. Systematic Development Strategy for Smart Devices Based on Shape-Memory Polymers. *Polym. Eng. Sci*. **9**, 496 (2017).
28. Xie, T. & Rousseau, I. A. Facile tailoring of thermal transition temperatures of epoxy shape memory polymers. *Polymer* **50**, 1852–1856 (2009).
29. Puig, J. et al. Epoxy Networks with Physical Cross-Links Produced by Tail-to-Tail Associations of Alkyl Chains. *Macromolecules* **42**, 9344–9350 (2009).
30. Leonardi, A. B. et al., Shape memory epoxies based on networks with chemical and physical crosslinks. *Eur. Polym. J.* **47**, 362-369 (2011).
31. Chang. N. et al. A manufacturing cost estimation method with uncertainty analysis and its application to perovskite on glass photovoltaic modules. *Prog. Photovolt: Res. Appl.* **25**, 390-405, (2017).
32. Material cost (Sigma Aldrich, 2018), http://sigmaaldrich.com.
33. Safety data sheet for Spiro-MeOTAD (Solaronix, 2018), https://www.solaronix.com/msds/MSDS_Spiro-OMeTAD.pdf.
34. Ma, B., Zhou, X., Wei, K., Bo, Y. & You, Z. Analysis of Preparation and Properties on Shape Memory Hydrogenated Epoxy Resin Used for Asphalt Mixtures. *Appl. Sci.* **7**, 523, (2017).
35. *Approval Standard for Rigid Photovoltaic Modules (FM 44787)* (FM Approvals, 2018); https://www.fmapprovals.com/products-we-certify/understanding-the-benefits/fm-approved-photovoltaic-modules.
36. Mathiak, G. et al. PV module damages caused by hail impact field experience and lab tests. *31st European Photovoltaic Solar Energy Conference and Exhibition*, 1915-1919, (2015).
37. *Solar Resource Information* (NREL, 2018); https://www.nrel.gov/rredc/solar_resource.html.
38. Hailegnaw, B., Kirmayer, S., Edri, E., Hodes, G. & Cahen, D. Rain on Methylammonium Lead Iodide Based Perovskites: Possible Environmental Effects of Perovskite Solar Cells. *J Phys. Chem. Lett.* **6**, 1543-1547, (2015).
39. Leyden, M. R., Jiang, Y. & Qi, Y. B. Chemical vapor deposition grown formamidinium perovskite solar modules with high steady state power and thermal stability. *J. Mater. Chem. A* **4**, 13125-13132, (2016).
40. Pantic, L. S. et al. The assessment of different models to predict solar module temperature, output power and efficiency for Nis, Serbia. *Energy* **109**, 38-48, (2016).
41. Espinosa, N., Zimmermann Y., Benatto, G. A. R., Lenz, M. & Krebs, F. C. Outdoor fate and environmental impact of polymer solar cells through leaching and emission to rainwater and soil. *Energy Environ. Sci.,* **9**, 1674-1680, (2016).
42. Serrano-Lujan, L. et al. Tin- and Lead-Based Perovskite Solar Cells under Scrutiny: An Environmental Perspective. *Adv. Energy Mater*. **5**, 1501119 (2015).
43. Hauck, M., Ligthart, T., Schaap, M., Boukris, E., & Brouwer, D. Environmental benefits of reduced electricity use exceed impacts from lead use for perovskite based tandem solar cell. *Renewable Energy,* **111**, 906-913, (2017).
44. Celik, I., Song, Z., Cimaroli, A. J., Yan, Y., Heben, M. J., & Apul, D, Life Cycle Assessment (LCA) of perovskite PV cells projected from lab to fab, *Sol. Energy Mater. Sol. Cells*, **156**, 157-169, (2016).
45. Celik, I., Song, Z., Phillips, A. B., Heben, M. J., & Apul, D. Life cycle analysis of metals in emerging photovoltaic (PV) technologies: A modeling approach to estimate use phase leaching, *J. Cleaner Prod*. **186**, 632-639 (2018).
46. Celik, I et al. Environmental analysis of perovskites and other relevant solar cell technologies in a tandem configuration, *Energy Environ. Sci*. **10**, 1874-1884, (2017).
47. Babayigit, A. et al. Assessing the toxicity of Pb- and Sn-based perovskite solar cells in model organism Danio rerio. *Sci. Rep.* **6**, 18721, (2016).
48. Babayigit, A., Ethirajan, A., Muller, M. & Conings, B. Toxicity of organometal halide perovskite solar cells. *Nat. Mater.* **15**, 247-251, (2016).
49. Holzhey, P. & Saliba, M. A full overview of international standards assessing the long-term stability of perovskite solar cells. *J. Mater. Chem. A* **6**, 21794-21808 (2018).
50. Rainfall intensity (Wikipedia, 2018); https://en.wikipedia.org/wiki/Rain.

Author contributions

Y. B. Q. conceived the idea, initiated and supervised the work. Y. J. and L. Q. designed the experiment, prepared the modules, tested the module breaking conditions and measured the Pb leakage amount. Y. J. performed the J-V measurements and water contact angle measurements. L. Q. carried out the DSC measurement. E. J. J. P. did the TG measurement. All authors contributed to writing the paper.

Data availability

The data that support the plots within this paper and other findings of this study are available from the corresponding author on reasonable request.

Acknowledgments

This work was supported by funding from the Energy Materials and Surface Sciences Unit of the Okinawa Institute of Science and Technology Graduate University, the OIST R&D Cluster Research Program, the OIST Proof of Concept (POC) Program, and JSPS KAKENHI Grant Number JP18K05266. We sincerely thank Dr. Yoshiteru Iinuma, the technician at OIST for ICP-MS measurements.

Competing interests

The authors declare no competing financial interests.